The Dynamics of A2125

Neal A. Miller – NASA Goddard Flight Center

Frazer N. Owen – National Radio Astronomy Observatory

John M. Hill – University of Arizona

William C. Keel – University of Alabama

Michael J. Ledlow – Gemini Observatory, Chile

William R. Oegerle – NASA Goddard Space Flight Center

Deposited 09/18/2018

THE DYNAMICS OF A2125

Neal A. Miller

NASA Goddard Space Flight Center, Laboratory for Astronomy and Solar Physics, Code 681,
Greenbelt, MD 20771; nmiller@stis.gsfc.nasa.gov

Frazer N. Owen[1]

National Radio Astronomy Observatory,[2] P.O. Box O, Socorro, NM 87801; fowen@aoc.nrao.edu

John M. Hill[1]

Large Binocular Telescope Observatory, University of Arizona, Tucson, AZ 85721; jhill@as.arizona.edu

William C. Keel[1]

Department of Physics and Astronomy, University of Alabama, Box 870324, 206 Gallalee Hall,
Tuscaloosa, AL 35487; keel@bildad.astr.ua.edu

Michael J. Ledlow[1]

Gemini Observatory, c/o AURA, Casilla 603, La Serena, Chile; mledlow@gemini.edu

and

William R. Oegerle[1]

NASA Goddard Space Flight Center, Laboratory for Astronomy and Solar Physics, Code 680,
Greenbelt, MD 20771; william.r.oegerle@nasa.gov

Received 2003 December 1; accepted 2004 June 10

ABSTRACT

We present 371 galaxy velocities in the field of the very rich cluster A2125 ($z \approx 0.25$). These were determined using optical spectroscopy collected over several years from both the WIYN 3.5 m telescope and NOAO Mayall 4 m telescope. Prior studies at a variety of wavelengths (radio, optical, and X-ray) have indicated that A2125 is a likely cluster-cluster merger, a scenario that we are able to test using our large velocity database. We identified 224 cluster galaxies, which were subjected to a broad range of statistical tests using both positional and velocity information to evaluate the cluster dynamics and substructure. The tests confirmed the presence of substructures within the A2125 system at high significance, demonstrating that A2125 is a complex dynamical system. Comparison of the test results with existing simulations strengthens the merger hypothesis and provides clues about the merger geometry and stage. The merger model for the system can reconcile A2125's low X-ray temperature and luminosity with its apparently high richness and might also explain A2125's high fraction of active galaxies identified in prior radio and optical studies.

Subject headings: galaxies: clusters: individual (A2125) — galaxies: evolution —
galaxies: kinematics and dynamics

Online material: machine-readable tables

1. INTRODUCTION

A2125 is a very rich cluster of galaxies (richness class 4; Abell et al. 1989) found at intermediate redshift ($z \approx 0.25$). It was identified as an active cluster in the Butcher & Oemler (1984) study, with a noted blue fraction of 0.19. This would suggest an increase in the star formation of A2125 galaxies relative to those found in low-redshift clusters, which typically have blue fractions ~0.03. Considerable effort has been expended to confirm this suggestion via radio continuum observations (Dwarakanath & Owen 1999; F. N. Owen et al. 2004, in preparation). The radio continuum emission at 20 cm for normal and starbursting spirals is strongly correlated with

far-infrared (FIR) emission (e.g., Helou et al. 1985; Yun et al. 2001). It is believed that the source of this correlation is massive stars, whose supernovae accelerate electrons that radiate synchrotron emission in galactic magnetic fields (for a review see Condon 1992). The same massive stars are the dominant source of FIR emission as they heat gas and dust in their parent molecular clouds. Indeed, analogous to the photometric results, A2125 was shown to have a large radio galaxy fraction implying an elevated level of star formation (Dwarakanath & Owen 1999). A companion study adding optical spectroscopy confirmed that the identified radio galaxies were cluster members and argued that the high blue/radio fraction was due to the dynamical state of A2125, which appears to be that of a cluster-cluster merger (Owen et al. 1999). Additional radio and optical observations have extended this result to much lower luminosities (F. N. Owen et al. 2004, in preparation), further underscoring the high level of activity in A2125. This activity includes a high fraction of active galactic nuclei (AGNs), as well as an excess of star-forming galaxies.

The interpretation of A2125 as a cluster-cluster merger is based on both its galaxy distribution (Owen et al. 1999) and its

---

X-ray structure (Wang et al. 1997, 2004). The Wang et al. (1997) X-ray observations were performed with the *ROSAT* PSPC and indicated a complex environment. This impression was strengthened by recent *Chandra* observations in Wang et al. (2004). Multiple peaks in the X-ray emission were identified, in addition to larger scale diffuse emission. The emission coinciding with the core of A2125 was shown to have an ellipticity of 0.25–0.33 (*Chandra* results, 90% confidence range) and a north-to-east position angle between $115°$ and $127°$. The X-ray emission corresponding to the core of A2125 was also noted to be clumpy. In conjunction with the low measured temperature of 3.2 keV, these findings indicated that A2125 was a dynamically complex system. Additional peaks in the X-ray emission outside the main body of A2125 were observed to the north, along with more diffuse extended emission to the southwest. This diffuse emission is of cooler temperature ($\sim$1 keV) and correlates with concentrations of spiral galaxies. It might thereby represent diffuse intergalactic gas associated with large-scale hierarchical structure formation. In total, the X-ray observations led to the interpretation of the entire system as a supercluster over 7 Mpc in extent. Interestingly, the X-ray ellipticity of the main body of A2125 was roughly perpendicular to the overall superstructure, leading the authors to suggest that the core of A2125 represented "an initial coalescence of subunits of comparable mass."

Consequently, there is much interest in a detailed dynamical assessment of A2125. The prior studies lacked large numbers of measured galaxy velocities with which to assess possible substructures and the overall merger environment, and we have undertaken a broad campaign of optical spectroscopy to remedy this. In this paper we report over 450 new velocity measurements of 371 galaxies in the field of A2125. The optical spectra were collected using several instruments, including the Hydra multifiber spectrograph on the WIYN 3.5 m telescope, multislit spectra collected using the Mayall 4 m telescope, and long-slit spectra taken with the RC spectrograph at the Mayall telescope (previously published in Owen et al. 1999). The galaxy velocities and positions were subjected to a collection of statistical tests in order to identify substructure in A2125 and quantify its significance. A2125 is shown to be a highly complex system, rich in substructure. Comparison of the test results with those determined for simulations indicates that the data are consistent with models of cluster-cluster mergers. In this interpretation, A2125 is viewed along an axis offset slightly from the merger axis and at an epoch within a few hundred million years of the time when the cores of the merging clusters have crossed.

We begin with a description of the spectroscopy database in § 2. Analysis of the resulting velocities is presented in § 3. In § 4 we assess the merger hypothesis by comparing the substructure tests with computer models and view the results in light of X-ray and radio investigations of the cluster. Our conclusions are briefly summarized in § 5. We have adopted the *WMAP* cosmology of $H_0 = 71$ km s^{-1} Mpc^{-1}, $\Omega_m = 0.27$, and $\Omega_\Lambda = 0.73$ for all distance-dependent calculations, meaning that $1''$ corresponds to about 3.8 kpc at A2125. The classical Abell radius ($R_A \equiv 1'.7/z$; Abell 1958) for the cluster is thereby 1.59 Mpc.

2. OBSERVATIONS AND DATA REDUCTIONS

2.1. *Multifiber Spectroscopy Using WIYN with Hydra*

2.1.1. *1996 Observations*

Observations of A2125 were performed by W. R. O. and J. M. H. using the Hydra multifiber spectrograph on the

TABLE 1
Summary of Observations

Field ID	Date	Exposures (s)	Instrument
H1..................	1996 Apr 16	6×1800	WIYN+Hydra
H2..................	1996 Apr 16	2×2400	WIYN+Hydra
	1996 Apr 17	4×2400	WIYN+Hydra
H3..................	1996 Apr 17	3×2580	WIYN+Hydra
	1996 Apr 18	4×2580	WIYN+Hydra
H4..................	1996 May 20	4×2100	WIYN+Hydra
	1996 May 21	2×2100	WIYN+Hydra
	1996 May 22	2×2100	WIYN+Hydra
1187..............	1998 May 27	2×1800	Mayall multislits
1188..............	1998 May 27	2×1800	Mayall multislits
1189..............	1998 May 27	2×1800	Mayall multislits
1191..............	1998 May 27	2×1800	Mayall multislits
1196..............	1998 May 28	2×1800	Mayall multislits
1197..............	1998 May 28	2×1800	Mayall multislits
1198..............	1998 May 28	2×1800	Mayall multislits
1199..............	1998 May 28	2×1800	Mayall multislits
1200..............	1998 May 28	2×1800	Mayall multislits
1190..............	1998 May 29	2×1800	Mayall multislits
1192..............	1998 May 29	2×1800	Mayall multislits
1193..............	1998 May 29	2×1800	Mayall multislits
1194..............	1998 May 29	2×1800	Mayall multislits
Q101..............	2000 Mar 30	4×2800	WIYN+Hydra (queue)
	2000 Apr 2	2×2800	WIYN+Hydra (queue)
Q102..............	2000 May 27	6×2800	WIYN+Hydra (queue)
Q103..............	2000 May 28	5×2800	WIYN+Hydra (queue)

WIYN 3.5 m telescope during a pair of observing runs in 1996. Three fiber configurations were observed during 1996 April 16–18, and a fourth was observed during 1996 May 20–22. Each run used the blue fibers (3''1) and a 400 line mm^{-1} grating blazed at 4000 Å. This produced wavelength coverage from about 4300 to 7500 Å at a resolution of 7 Å. Each configuration was observed multiple times to reject cosmic rays and produce high signal-to-noise spectra. Total exposure times varied depending on observing conditions but ranged from 3 to 5 hr (see the summary in Table 1).

Calibration frames were taken using standard methods. At least 20 bias frames were collected on each night, as well as at least three flat fields per fiber configuration. Wavelength calibration was achieved via observation of CuAr lamps, performed both before and after science observations of a given fiber configuration. The wavelength solutions typically produced an rms residual less than 0.15 Å as determined from about 45 lines. Of the 96 available fibers per configuration, typically around 30 were assigned to random locations to produce a good-quality sky spectrum.

Each science exposure was reduced individually, with the set of exposures for a given fiber configuration then combined to produce the final spectra. The standard IRAF tasks within the NOAO HYDRA package were used to produce the final wavelength-calibrated, sky-subtracted spectra for each exposure. The set of exposures corresponding to a given fiber configuration were then median combined after weighting by their modes (as defined in a region between 5000 and 5500 Å, chosen to avoid strong emission and absorption features in cluster galaxies).

Measurement of galaxy velocities proceeded along one of two paths. First, the spectra were cross-correlated against a collection of velocity standards (using the IRAF RV package; see Tonry & Davis 1979). These included spectra of the

nearby galaxies NGC 3379 (assumed velocity 922 km s^{-1}), NGC 7331 (819 km s^{-1}), M31 (-297 km s^{-1}), M32 (-200 km s^{-1}), and a bright elliptical in A779 (6877 km s^{-1}, determined from cross-correlation with the other templates and observed multiple times), plus standard stars HD 52071 (94.7 km s^{-1}) and BD $+25°3190$ (-49.5 km s^{-1}). The velocity standard spectra (hereafter "template" spectra) were collected over several years using a variety of spectrographs at resolutions comparable to the present observations. In total, the template list included 22 spectra. Cross-correlation velocities for each observed galaxy were then determined from the velocities derived using each of the 22 templates. First, the average of the velocities was determined (weighted by the R-values, where R is a measure of the goodness of fit defined as the ratio of the height of the peak in the cross-correlation to that of the average peak; see Tonry & Davis 1979) and outliers were clipped ($\pm 3\ \sigma$). The dispersion in the remaining velocities was required to be less than 115 km s^{-1}, and we also required that the R-values were greater than 2.5. Finally, we required that at least 60% of the templates produced acceptable velocities given these restrictions. Initial errors were based on the weighted average R-value, such that the error equals $280(1+R)^{-1}$ km s^{-1} (see Tonry & Davis 1979; Hill & Oegerle 1998). The final error represents this value added in quadrature with an additional uncertainty of 40 km s^{-1} (see § 2.3).

The spectra were also inspected by eye by two of us (N. A. M. and F. N. O.) independently to confirm the results. In addition to confirmation of cross-correlation velocities, many emission-line spectra were identified. For these galaxies, we fitted Gaussian profiles to up to 11 emission lines typically observed in star-forming galaxies and AGNs: [O II] $\lambda3727$, Hγ $\lambda4340$, Hβ $\lambda4861$, [O III] $\lambda4959$, [O III] $\lambda5007$, [O I] $\lambda6300$, [N II] $\lambda6548$, Hα $\lambda6563$, [N II] $\lambda6583$, [S II] $\lambda6716$, and [S II] $\lambda6731$. Velocities were determined for each detected line, and a net galaxy velocity was derived from these via a simple average (requiring that at least two emission lines be measured). The heliocentric correction was then applied to arrive at the final emission-line velocity. To evaluate the errors, we determined the dispersion in the line measurements for each galaxy. As this quantity is somewhat dependent on the number of measured lines (e.g., a galaxy with only two measured lines may have a much lower associated dispersion than a strong emission-line galaxy with 10 lines), we calculated the average dispersion over all emission-line galaxies, arriving at a value of 39 km s^{-1}. This represents the combination of various error terms including errors in measurement of line positions, wavelength calibration errors (which should be about 10 km s^{-1} based on the rms residual obtained from the wavelength solution), and gas motions within the galaxies. We therefore adopted 40 km s^{-1} as the error in our velocities determined from emission lines.

Final velocities were then adopted based on the cross-correlation and emission-line values. For galaxies proving to be cluster members (see below), these observed heliocentric corrected velocities (cz) may be found in Table 2. For non-cluster members (foreground and background galaxies and quasars), the heliocentric redshifts may be found in Table 3. In general, we used the emission-line values whenever they were available. For several cases in which the lines were weak or noisy, we instead used the cross-correlation values. These are marked in Tables 2 and 3 with the noted emission lines offset in parentheses. Note that in nearly all cases in which both an emission-line and a cross-correlation velocity were available, the two velocities were consistent within about 150 km s^{-1}. A

TABLE 2
Cluster Velocity Data

R.A.	Decl.	cz	Error	Lines	Source
15 38 13.9	+66 13 06	74199	81	⋯	W00
15 39 02.0	+66 05 24	77196	81	⋯	W00
15 39 08.8	+66 08 54	73449	49	⋯	W00
15 39 22.2	+66 12 42	73419	40	[O II], [O III]	W00
15 39 23.1	+66 19 58	73068	40	[O II], Hβ	W96

Notes.—Units of right ascension are hours, minutes, and seconds, and units of declination are degrees, arcminutes, and arcseconds. All coordinates are J2000.0, and heliocentric velocities (note that these are not relativistically corrected and are therefore cz) and errors are in km s^{-1}. Emission lines used in determination of the reported velocities are indicated. When these are enclosed in parentheses, the velocity was determined through cross-correlation but the noted emission lines were also detected at a consistent velocity. The abbreviations for the data sources are as follows: W96 = WIYN Hydra 1996; W00 = WIYN Hydra 2000; M98 = Mayall 1998. Table 2 is published in its entirety in the electronic edition of the *Astrophysical Journal*. A portion is shown here for guidance regarding its form and content.

small number of cross-correlation velocities with low R-value were adopted in specific cases in which a single emission-line measurement (usually [O II]) confirmed the cross-correlation value.

2.1.2. *2000 Observations*

Additional spectroscopy using Hydra on the WIYN telescope was performed in the queue observing mode over several nights from 2000 March through May (see Table 1). These used the red cables (2″ fibers) and the 316 line mm^{-1} grating blazed at 7°, providing wavelength coverage from $\sim$4300 to $\sim$9150 Å at $\sim$6 Å resolution. Three fiber configurations each consisting of $\sim$65 target galaxies were observed in five or six exposures each of 2800 s duration. Most of the remaining fibers were used to create a sky spectrum for data reduction. In addition to the science exposures, CuAr wavelength calibration frames were interspersed along with observations of velocity and spectrophotometric standards. Zeros, dome flats, and sky flats were also obtained on each night.

The data reduction and determination of velocities were similar to those for the 1996 data. The procedure for determining the cross-correlation velocities differed slightly from that outlined above. Five template spectra, corresponding to M31, M32, NGC 3779, NGC 7331, and HD 132737 (assumed velocity of -24 km s^{-1}), were each run interactively with the individual spectra. Regions for the correlations were chosen on a case-by-case basis to emphasize stronger absorption features such as the 4000 Å break, with the best fit (i.e., highest R-value) being adopted as the velocity for a given galaxy. Velocity errors were then determined in the same manner as for the 1996 WIYN data.

2.2. *Multislit Spectroscopy at* 4 m *Mayall Telescope*

The 4 m Mayall Telescope was used for spectroscopic observations of A2125 by W. C. K., F. N. O., and M. J. L. on three nights from 1998 May 27 to 29 (Table 1). These observations were performed using 13 custom-made multislit masks, each consisting of between eight and 13 2″.5 slits centered on target galaxies. The primary motivation of these observations was to obtain spectra of galaxies with radio emission (see F. N. Owen et al. 2004, in preparation), with additional slits placed on galaxies with $m_R \leq 20$. The RC

TABLE 3
Noncluster Redshifts

R.A.	Decl.	z	Error	Lines	Source
15 37 56.1	+66 27 36	0.2049	0.0003	...	W00
15 38 12.4	+66 14 05	0.4373	0.0001	[O ii], [O iii]	W00
15 39 00.4	+65 59 48	0.2878	0.0002	...	W00
15 39 20.1	+66 14 28	0.3365	0.0003	...	W00
15 39 20.1	+65 57 23	1.9010	0.0010	C iv, O iii], C iii]	W00

Notes.—Units of right ascension are hours, minutes, and seconds, and units of declination are degrees, arcminutes, and arcseconds. All coordinates are J2000.0, and reported redshifts and errors are heliocentric. Emission lines used in determination of the reported redshifts are indicated. When these are enclosed in parentheses, the redshift was determined through cross-correlation but the noted emission lines were also detected at a consistent redshift. The abbreviations for the data sources are as follows: W96 = WIYN Hydra 1996; W00 = WIYN Hydra 2000; M98 = Mayall 1998. Table 3 is published in its entirety in the electronic edition of the *Astrophysical Journal*. A portion is shown here for guidance regarding its form and content.

spectrograph was used along with grating KPC-10A (316 lines mm^{-1}, blazed at 4000 Å), providing a resolution of ∼7 Å and coverage from 4000 past 9200 Å. Each mask was observed for a total exposure time of 1 hr, split into two 30 minute exposures to facilitate rejection of cosmic rays. Flux calibration was achieved through observation of standard stars through slits of the same width, including standard stars viewed through slits from the actual science multislit masks. Data reduction and determination of galaxy velocities were achieved in the same manner as that applied to the 2000 WIYN data.

2.3. *Additional Data and Combination of Velocities*

In addition to the velocity data described above, we have included the velocity data from Owen et al. (1999). These were obtained using a long slit on the KPNO Mayall 4 m telescope with the RC spectrograph. Most of these galaxies have been reobserved by at least one of the above spectroscopic campaigns, meaning that only three velocities (two of which are cluster galaxies) are added to the data from this source. In total, there are 374 galaxies in our database, including 371 listed in Tables 2 and 3. Many galaxies have spectroscopy results from multiple observing runs, meaning that the two tables contain a total of 454 entries.

Visual inspection of the spectra also identified a handful of quasars. These have been noted in Table 3, along with their redshifts and comments indicating the emission features upon which such measurements are based. The broad emission lines make precise determination of redshifts difficult, so we have arbitrarily assigned an error of $\Delta z = 0.001$ (300 km s^{-1}) to these redshifts.

With many galaxies being the targets of multiple observing runs, we explored possible offsets in our derived velocities. We adopted the 1996 WIYN Hydra observations as a benchmark and compared the velocities obtained from these observations with the velocities obtained from the other observations (the 2000 WIYN Hydra observations and the 1998 Mayall observations). These comparisons were further split into velocities determined by cross-correlation and velocities determined by locations of emission lines. The emission-line velocities in common were consistent for each data set (mean difference between 2000 WIYN data and 1996 WIYN data of −7 km s^{-1} for 17 galaxies, mean difference between 1998 Mayall data and 1996 WIYN data of 12 km s^{-1} for 10 galaxies). The velocities determined via cross-correlation were also generally consistent, with the 2000 WIYN velocities an average of 51 km s^{-1} greater than the 1996 WIYN velocities (17 objects in common)

and the 1998 Mayall velocities an average of 15 km s^{-1} less than the 1996 WIYN velocities (based on 24 common objects). Differences as small as these can easily result from sampling different portions of the target galaxies through combinations of astrometry, pointing, and aperture size.

We further tested possible offsets using velocity standard star observations. Typically, a velocity standard star was observed on each night of the observing runs. Velocities for these standard stars were determined via cross-correlation using the various template velocity standard spectra. The mean velocity for a given standard star, determined from the full set of template spectra, was usually within 15 km s^{-1} of the cataloged velocity. The full spread in velocities determined from the various templates was ≲70 km s^{-1}, with a typical dispersion around 20 km s^{-1}. Rather than apply any zero-point shifts to velocities determined from data collected on specific nights and observing runs (none of which would be statistically significant), we have elected to include an additional error of 40 km s^{-1} (added in quadrature) to the reported galaxy velocities.

In compiling our final velocity list for dynamical analysis, we prioritized the observations as follows. If a velocity obtained from the 1996 WIYN observations was available for a given galaxy, it was adopted. If a galaxy was unobserved by the 1996 WIYN observations, we used its 2000 WIYN velocity (if available), followed by any 1998 Mayall velocity and lastly by any Owen et al. (1999) velocity. This hierarchy is largely governed by numbers and is meant to maintain as consistent a velocity database as possible.

With spectroscopy data coming from four separate sources, it is useful to investigate possible bias in our sampling of cluster galaxies (e.g., obtaining relatively more velocities for some portions of the cluster than for others). Fortunately, this is mitigated by the large (60′ diameter) field of view of WIYN+Hydra, which equates to nearly 7 Mpc at the redshift of the cluster. In Figure 1 we plot the positions of all galaxies for which we have spectra. It can be seen that our spatial sampling is relatively uniform, particularly by noting the distribution of background galaxies (*open triangles in the figure*). Optical images of the cluster, particularly those with high resolution, often reveal tight groupings of galaxies (F. N. Owen et al. 2004, in preparation). Limitations on fiber spacing with Hydra (37″) mean that any single fiber configuration will miss some galaxies. However, since seven different fiber configurations were observed (four in 1996, three in 2000), this effect is lessened. Overall, the net effect of missing a few
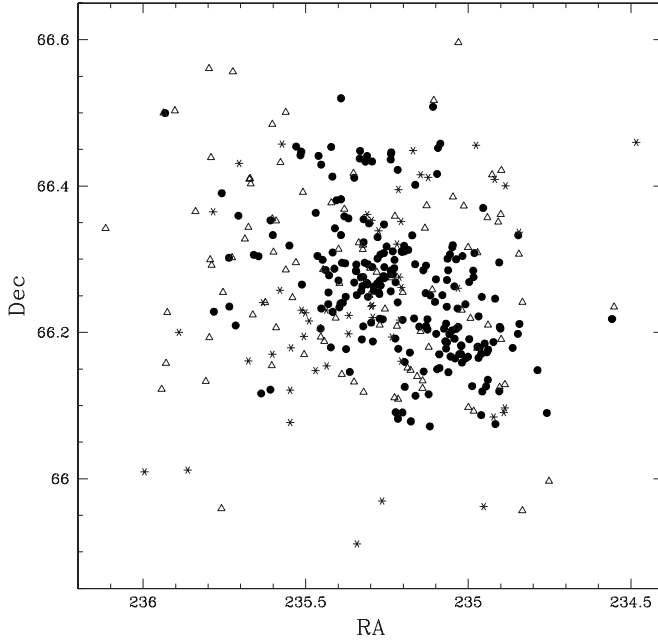
Fig. 1.—Coded positions of all galaxies in the spectroscopic database. Cluster members are represented by filled circles, background galaxies by open triangles, and foreground galaxies by asterisks. The relative uniformity of sampling is indicated by the fairly even distribution of background galaxies.

Fig. 2.—Histogram for all data with $cz < 175,000$ km s^{-1}, using a bin size of 400 km s^{-1}. The location of A2125 is easily apparent and is detailed in the inset histogram. The binning for the inset is 200 km s^{-1}.

galaxies in tight groupings should be minimal in performing the dynamical assessments. In fact, missing spectra for some galaxies in tight groups would result in less pronounced evidence for substructure than is actually present.

3. ANALYSIS: TESTS OF SUBSTRUCTURE

A histogram of the velocity data is presented in Figure 2. A2125 is easily seen as the single strong peak in the velocity distribution. In all, there are 224 cluster galaxies as identified via 3 σ clipping of the velocity data (Yahill & Vidal 1977). The calculated biweight location and scale (see Beers et al. 1990) are $73,897 \pm 74$ ($z = 0.2465$) and 1113^{+57}_{-49} km s^{-1}, respectively. These numbers have been corrected for measurement errors (see Danese et al. 1980), and the dispersion was calculated from relativistically corrected velocities (which we use for all subsequent dynamics calculations). We adopt the biweight location as our cluster systemic velocity and the biweight scale as our cluster velocity dispersion for the remainder of this discussion. Note that the "nonrobust" calculations of the mean and dispersion yield $73,995 \pm 96$ and 1150^{+59}_{-51} km s^{-1}, similar to the robust quantities.

The 224 cluster galaxies were subjected to a battery of statistical tests to evaluate potential substructure. These included tests performed exclusively on the velocity data (the "ROSTAT" package of Beers et al. 1990) and tests on the galaxy positional data both with and without velocity information (for a complete listing and description of all tests, see Pinkney et al. 1996, hereafter P96). The advantages to using a battery of statistical tests are noted in P96. Essentially, each test provides a different perspective on the dynamical state of the cluster, and taken collectively they often complement one another. Understanding a set of results is aided greatly by comparison with numerous N-body simulations.

The tests performed exclusively on the velocity data (one-dimensional tests) generally compare the distribution to that of a Gaussian and are presented in Table 4. Since the
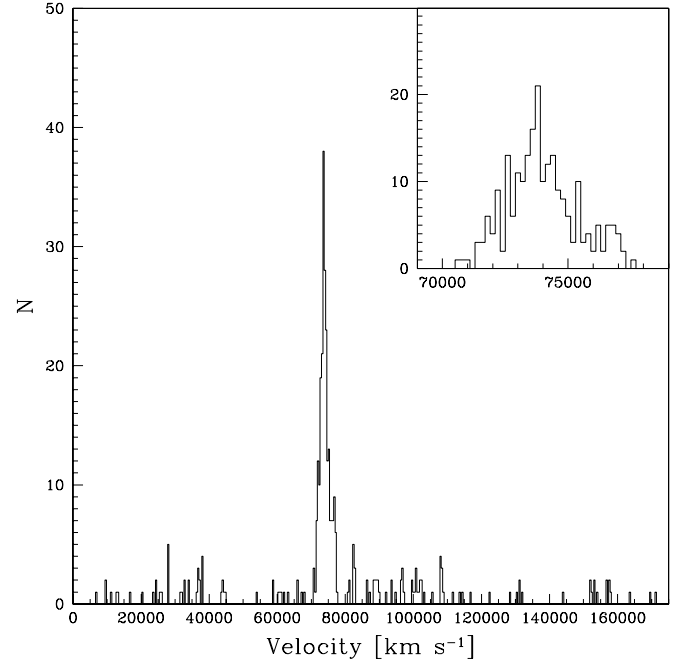
computational algorithms in the ROSTAT package that are used to determine the significance for the B_1 and B_2 statistics (B_1 and B_2 are the canonical estimators of skewness and kurtosis and represent the third and fourth moments of the velocity distribution) fail for large N, we have estimated their significance via 40 randomly drawn subsets (with $N = 150$) of the full data set. Most of the one-dimensional tests indicated significant non-Gaussian behavior of the velocity histogram. Qualitatively, this may be understood by inspection of Figure 2. In particular, the cluster histogram has a "tail" at higher velocity. This produces significant skewness to the distribution but does not make it overly kurtotic (e.g., the cluster distribution is more skewed than a Gaussian at better than 95% confidence based on the B_1 statistic, yet consistent with a Gaussian in the sense of kurtosis based on the B_2 statistic). Consistent with the visual interpretation, combinations of the statistics indicate that the distribution has more counts to the higher velocity side of the mean and similarly that the long tail identified by the tests resides on this side.

Similarly, tests performed on the positional data both with and without the associated velocities produced strong evidence for substructure. Table 5 presents the nine tests performed and their results. With the exceptions of the angular separation test (AST; West et al. 1988) and the ϵ test (Bird 1993), all indicate highly significant substructure (at $\geq 99.7\%$ confidence, as determined via 1000 Monte Carlo simulations). As an example, in Figure 3 we present the graphical representation of the Δ test (Dressler & Shectman 1988). This test calculates local deviations from the systemic velocity (v_{sys}) and dispersion (σ) of the entire cluster:

$$\delta_i^2 = \frac{N}{\sigma^2} \left[\left(v_{local} - v_{sys}\right)^2 + \left(\sigma_{local} - \sigma\right)^2 \right]. \quad (1)$$

Here N is the number of galaxies that defines the local environment around galaxy i, taken to be $N = 11$ in the original

TABLE 4
NORMALITY TESTS FOR A2125

Test	Statistic	Significance
A	0.784	[a]
U	4.840	0.000
W	0.965	0.001
B_1	0.334	0.045[b]
B_2	2.762	0.324[b]
B_1B_2 Omni	3.343	0.184[b]
I	0.980	0.150[c]
KS	1.017	0.025[d]
V	1.714	0.010
W^2	0.214	0.004
U^2	0.185	0.005
A^2	1.342	0.002
DIP	0.017	0.030
AI	0.109	[a]
TI	1.252	[a]

NOTES.—The significance represents the probability that the distribution is consistent with a Gaussian. Thus, a low number indicates likely non-Gaussian behavior.

[a] The significance for these tests cannot be determined analytically. For comparison purposes, the AI test statistic for a Gaussian is equal to 0.0 and for TI it is equal to 1.0. See Bird & Beers (1993) for more information on the AI and TI tests.

[b] Based on the results for 40 $N = 150$ data sets drawn at random from the full $N = 224$ set of velocities (see text). The dispersions in these values (i.e., the biweight scales) were 0.041 for B_1, 0.122 for B_2, and 0.135 for the B_1B_2 Omni test. In each case, the test statistic derived from the 40 $N = 150$ data sets was nearly identical to that derived for the full $N = 224$ data.

[c] This is the default value for a nonsignificant deviation for the implementation of this test (see P96). Note that all 40 $N = 150$ randomly drawn subsets of the full velocity list yielded significance values of 0.15, indicating no significant deviation from a Gaussian. The I test is normally evaluated and compared to I_{90} to determine whether a distribution is non-Gaussian; distributions are considered consistent with a Gaussian if $I < I_{90}$. For the A2125 velocities, $I_{90} = 1.024$.

[d] The significance values for this implementation of the KS test are restricted to 0.25, 0.15, 0.10, 0.05, 0.025, and 0.01. Using the 40 randomly drawn $N = 150$ subsets, the robust mean significance is 0.055 with a dispersion of 0.086.

TABLE 5
MULTIDIMENSIONAL SUBSTRUCTURE TESTS FOR A2125

Test	Dimensionality	Significance	Reference
Fourier elongation	2D	0.000	1
β	2D	0.000	2
Angular separation	2D	0.063	2
Lee	2D	0.001	3
Lee	3D	0.001	1
Δ	3D	0.003	4
ϵ	3D	0.130	5
α	3D	0.000	6
α variant	3D	0.000	1

NOTES.—Implementations of all tests are described in P96 and generally follow the prescriptions for the tests as set forth by the original authors. One minor exception is the number of nearest neighbors used, which was frequently 10 in the original tests (e.g., the Δ and α tests) but set to $N^{1/2}$ in the P96 code [hence, $(224)^{1/2} = 14.97$ and the tests used the 15 nearest neighbors]. Significance values are determined from 1000 Monte Carlo simulations.

REFERENCES.—(1) P96; (2) West et al. 1988; (3) Fitchett 1988; (4) Dressler & Shectman 1988; (5) Bird 1993; (6) West & Bothun 1990.
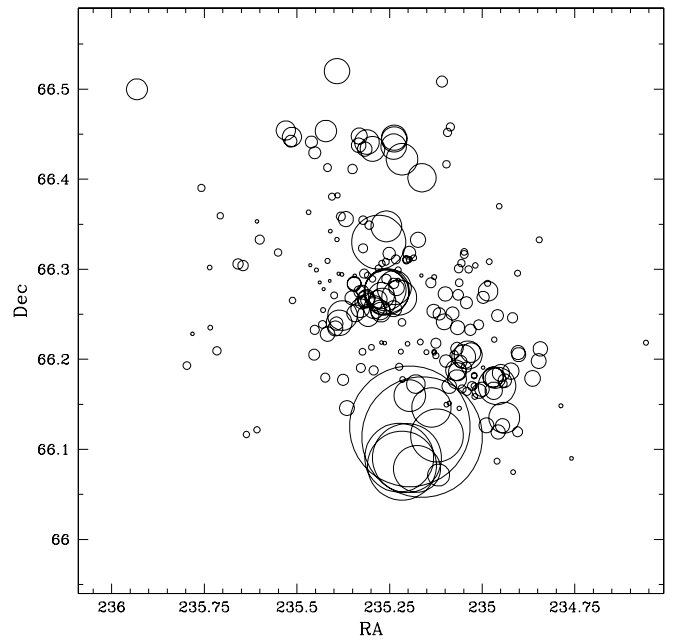

FIG. 3.—Dressler-Shectman plot for A2125. Each galaxy is plotted by a circle with the diameter of the circle proportional to e^δ.

formulation of the test (i.e., a given galaxy and its 10 nearest neighbors). For our calculations, we adopt $N = 15$ (the square root of the total number of galaxies) as in P96. The sum of δ over all cluster members represents the actual test statistic, Δ, and is approximately equal to the total number of cluster galaxies in the case of no substructure. Higher Δ indicate groupings that deviate from the cluster as a whole in either their mean velocity or dispersion (or both). For reference, $\Delta = 309.9$ for our cluster sample of 224 galaxies. The significance is evaluated by Monte Carlo shuffles of the velocities while holding the positions fixed; this is the null hypothesis that there is no relationship between position and velocity. Graphically, each galaxy in the cluster may be represented by a circle with radius proportional to e^{δ_i}. Thus, collections of larger circles indicate regions of substructure. Such regions are readily apparent in Figure 3, particularly to the northeast and southwest (and also slightly to the north of the cluster center).

In an attempt to identify substructures and determine which galaxies compose these substructures, we applied the KMM algorithm (see Ashman et al. 1994). This algorithm divides a system into a specified number of components and calculates the Gaussian distance (using both positions and velocities) of each galaxy to each component.[3] The galaxies are assigned to their nearest component, new means and dispersions for the positions and velocities of each component are calculated, and the procedure is repeated. The algorithm converges when the assignments are stable. In addition to the assignments, the probability that a given assignment is accurate may be assessed through the Gaussian distances of that galaxy to each component. For example, if a galaxy were equidistant to two components, its assignment would only imply 50% confidence. It should be stressed that the algorithm is statistical and does not necessarily imply association with a real physical

[3] The "Gaussian distance" for a given galaxy to component i is defined as $f_i = \exp\left\{-[(\alpha - \bar{\alpha}_i)/2\sigma_{\alpha_i}]^2 - [(\delta - \bar{\delta}_i)/2\sigma_{\delta_i}]^2 - [(v - \bar{v}_i)/2\sigma_{v_i}]^2\right\}$, where $\bar{\alpha}_i$ is the mean and σ_{α_i} is the dispersion in right ascension for galaxies in component i, etc. See Miller et al. (2003) for additional details.

TABLE 6
POSSIBLE SUBSTRUCTURES FROM KMM RUNS: VELOCITY

| | COMPONENT 1 | | | COMPONENT 2 | | | COMPONENT 3 | | |
FITTED COMPONENTS	N	C_{BI} (km s^{-1})	S_{BI} (km s^{-1})	N	C_{BI} (km s^{-1})	S_{BI} (km s^{-1})	N	C_{BI} (km s^{-1})	S_{BI} (km s^{-1})
1......................................	224	73897	1113	...	...	...	...	...	...
2......................................	170	73425	712	54	75970	603	...	...	...
3......................................	136	73656	479	58	75889	623	30	71926	362

NOTE.—C_{BI} and S_{BI} refer to the robust estimates of the mean and dispersion for each fitted component.

substructure. Any number of components may be specified by the user, and the algorithm will attempt to apportion the data into those components. In some cases, the algorithm either will not converge or will remove nearly all galaxies from a given component, indicating that the specified component is not viable.

Based on the observation that the velocity histogram had a long tail at higher velocities, our first KMM run divided the cluster into two components, a primary and a higher velocity subcluster to the southwest. Noting the multiple regions for substructure in the graphical representation of the Δ test (Fig. 3), we proceeded to a three-component fit. This fit kept the higher velocity subcluster to the southwest largely intact and split off a lower velocity system to the northeast. This same general impression is obtained from an adaptively smoothed distribution of the galaxy surface density, as shown in Figure 5 of Owen et al. (1999). Details of these KMM runs are provided in Tables 6 and 7, and the results of the three-component fit are depicted in Figures 4 and 5.

A slight digression on the validity of the KMM assignments is in order. The original astronomical application of KMM by Ashman et al. (1994) was to detect bimodality in univariate data sets. For this purpose, and assuming that the data are split into two components of equal dispersion but different mean, the authors found KMM to be relatively insensitive to input parameters. As might be expected, we have found through extensive testing that addition of variables largely removes this independence on input conditions. Clearly, adding two additional variables (for position) and relaxing the constraint that different components have common dispersions in a given variable expands the set of possible solutions. For example, with carefully chosen input parameters we were able to produce a two-component fit that largely ignored velocity and separated the cluster into a main component and a southwest clump, as well as a three-component fit that largely ignored

position and subdivided the higher velocity galaxies into two components. The merits of these various solutions are difficult to debate; Ashman et al. (1994) note that the significance at which an additional substructure improves the fit to the data is difficult to determine in all but the fairly simple case of a single variable decomposed into two components of equal dispersion but different mean. It is largely for these reasons that we did not extend the KMM analysis to more than three components. We note here that other solutions exist, but the two we discuss were driven by the substructure test results and in particular by the locations of substructure indicated by the Δ test (Fig. 3).

The KMM assignments enable us to revisit Figure 3, the Dressler-Shectman bubble plot (refer also to Fig. 4). Three regions of possible substructure are identified from the plot as collections of larger circles: one to the northeast, one to the southwest, and one slightly north of the cluster core. These may be caused either by groupings of galaxies at a velocity differing from the cluster as a whole or by groupings of galaxies with local dispersions differing from the cluster as a whole (refer to eq. [1]). The possible northeast substructure has larger δ-values primarily because its galaxies are at a lower velocity than the cluster. This corresponds to the lower velocity component identified in the KMM runs fitting more than two substructures. The possible southwest substructure has larger δ-values because (1) its galaxies have a higher local systemic velocity than the remainder of the cluster and (2) the higher velocity galaxies are seen in projection with galaxies at the same general velocity as the cluster, thus increasing the velocity dispersion among nearest neighbors (in particular, note the concentration of higher velocity galaxies to the southeast of the main southwest clump). This region corresponds to the higher velocity component identified in the KMM runs. Finally, the higher local δ-values just to the north of the cluster core are the result of large local velocity dispersion. This is

TABLE 7
POSSIBLE SUBSTRUCTURES FROM KMM RUNS: POSITION

| | COMPONENT 1 | | COMPONENT 2 | | COMPONENT 3 | |
FITTED COMPONENTS	R.A. (J2000.0)	Decl. (J2000.0)	R.A. (J2000.0)	Decl. (J2000.0)	R.A. (J2000.0)	Decl. (J2000.0)
1......................................	15 40 52	66 15 39	...	...	...	...
2......................................	15 40 53	66 16 23	15 40 50	66 13 18	...	...
3......................................	15 40 43	66 15 30	15 40 53	66 13 39	15 41 35	66 19 27

NOTES.—Units of right ascension are hours, minutes, and seconds, and units of declination are degrees, arcminutes, and arcseconds. Coordinates presented refer to the mean centers for each component. The errors in these means range from about one to several arcminutes.
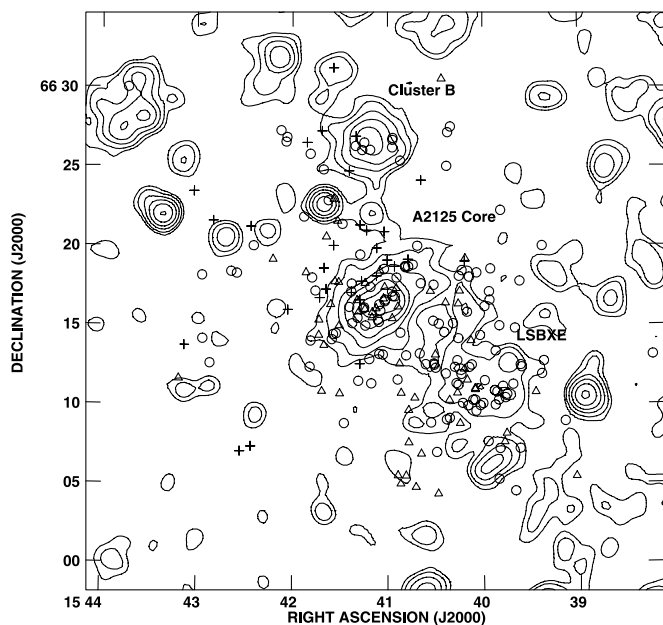
FIG. 4.—Distribution of A2125 galaxies based on KMM fitting of three substructures, overlaid on X-ray contours from the smoothed *ROSAT* PSPC image. X-ray labels, as presented in Wang et al. (1997), are located above and to the right of the corresponding features. The open triangles represent galaxies from the high-velocity component, the plus signs represent the low-velocity component, and the circles represent the main cluster (refer also to Fig. 5 for the velocity histograms).
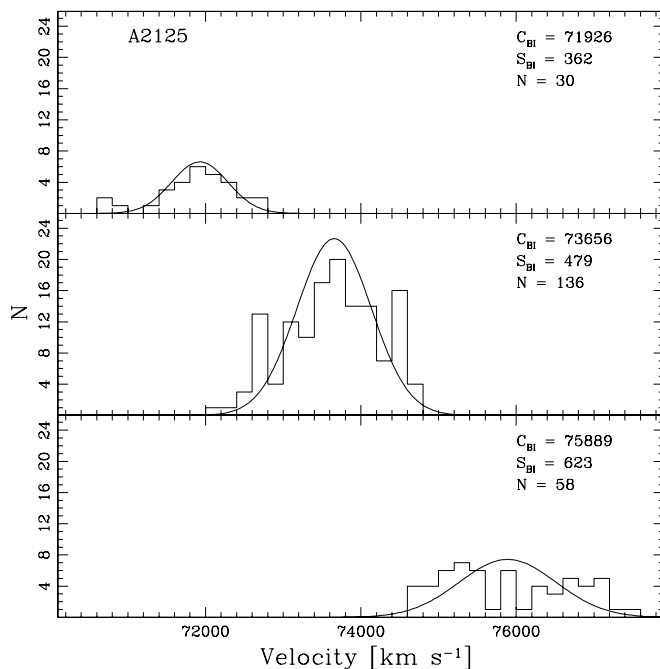

FIG. 5.—Velocity histograms for the KMM fitting of three substructures (see Fig. 4 for positional information). Gaussians with mean and dispersion set to the biweight location and scale of each component are overplotted.

caused by the superposition of galaxies from the low-velocity substructure, the high-velocity substructure, and the main body of the cluster.

4. DISCUSSION

4.1. *The Dynamical State of A2125*

The above analysis indicates that A2125 possesses very strong evidence for substructure. What is the cause of this behavior? There are several possible interpretations. It is possible that we are simply viewing a projection of multiple clusters. The velocity separation of the main cluster and the higher velocity system implies a physical separation of $\sim$45 Mpc, assuming that the difference is simply due to the Hubble flow. Their close alignment along the line of sight would then be fairly remarkable. Bahcall et al. (2003) used early Sloan Digital Sky Survey data to compile a cluster catalog out to $z \sim 0.3$ and from these data determined an estimate of the space density of galaxy clusters. Should clusters be distributed randomly, this space density implies that the probability of any two clusters being seen at an angular separation of less than or equal to that implied by the KMM fits is 2.2%. If we restrict this further to clusters at the redshifts implied by the KMM fits, the probability is only 0.1%. Of course, this is a gross estimate; it ignores the reality of large-scale structure (which would increase the probability of such an alignment) but also does not take into account the richness of the clusters (the SDSS catalog includes substantially poorer clusters, so the chance of two clusters as rich as implied by the velocity dispersions in Table 6 being aligned would be lower). In addition, a simple superposition does not entirely fit with the X-ray data. Figure 4 includes X-ray contours derived from the smoothed *ROSAT* data. The cluster galaxies reported in this study match reasonably well with the X-ray features, with concentrations tracing the core of A2125 and the more diffuse X-ray emission to the southwest (labeled

"LSBXE" after Wang et al. 1997). Although there is substantial overlap in the positional distributions of galaxies in the KMM fits, a rough mapping has the higher velocity system associated with the southwest X-ray emission. But as noted in Wang et al. (1997, 2004), this region is not simply explained as a single cluster or group: it is too diffuse to be a virialized cluster (and is composed primarily of spiral galaxies), and although its X-ray temperature ($\sim$1 keV) is representative of groups, its luminosity (over 10^{43} ergs s^{-1}) is in excess of typical group luminosities by an order of magnitude. Our velocity data also indicate a much higher dispersion than would be expected for a single poor cluster or group and similarly that the velocities are poorly fitted by a Gaussian (Fig. 5, although the Gaussian hypothesis for this component cannot be rejected via either the I or KS tests). Thus, these X-ray papers favor that the diffuse X-ray emission to the southwest arises from hot intergalactic gas in a hierarchical structure including multiple groups. Presumably, this structure is oriented roughly along our line of sight and connects to the core of A2125.

Another possibility is that we are witnessing a cluster-cluster merger. This interpretation is based largely on comparison of the substructure test results with the N-body simulations of cluster-cluster mergers presented by P96. In general, the one-dimensional tests (i.e., those performed using only the galaxy velocities) are excellent indicators of mergers viewed near core passage when the relative velocity between the merging partners is greatest. Of course, this requires that the merger not be viewed orthogonal to the merger axis. Conversely, the two-dimensional (positions only) tests perform best at early epochs of mergers and when the system is viewed orthogonal to the merger axis, thereby maximizing the positional separation of the merging partners. The three-dimensional tests combine the strengths and weaknesses of their lower dimensional counterparts.

Such consistently strong indications of substructure as are found in A2125 (refer to Table 5) are fairly rare in the sim-

ulations. Even so, the results are generally consistent with either of two possibilities. The first is the earlier stages of a merger (up to 2 Gyr prior to core passage) in which the positional separation of the two components is large and consequently the system is viewed closer to orthogonal to the merger axis. The second possibility is a merger seen near the epoch when the cores of the respective clusters have become coincident and with a viewing angle more closely aligned with the merger axis (within about $30°$). Since the latter possibility is the same as that obtained from the one-dimensional substructure tests, this scenario best matches the A2125 data. It is also interesting to note that the two multidimensional tests that do not suggest overly strong evidence for a merger are the two least sensitive tests identified by the simulations. These are the AST (West et al. 1988) and the ϵ test (Bird 1993). The AST looks for substructure in the form of small angular separations where the angle between any two galaxies is defined using the cluster centroid as the vertex. It therefore performs best when subclusters are well separated, a condition that fails around the time of core passage or if the system is viewed along the merger axis. The ϵ test calculates the projected mass estimator in the vicinity of galaxies using their nearest neighbors. Regions of substructure have lower projected mass estimates than the global mass estimate, and the significance of this deviation is tested via Monte Carlo shuffles of the data. Although the ϵ test is sensitive to mergers, it is most sensitive for times well after core passage (P96).

If the merger hypothesis is correct, whether the system is being viewed before or after core passage is dependent on the viability of the lower velocity component in the KMM fits. P96 note that the difference in the velocity dispersions of the two components (for ease of reference, hereafter called the primary and the subcluster) is a good diagnostic of the timing of the merger (see their Table 9). Prior to core passage, the velocity dispersion of the primary is larger than that of the subcluster simply because of its greater mass. As the subcluster merges with the primary, it is dispersed and thereby obtains the larger dispersion. In the two-component KMM fit, the subcluster has a slightly lower velocity dispersion and would then indicate that the system is being viewed shortly before core passage (see Table 6). Removing the lower velocity galaxies from the primary when going to a three-component fit reduces the dispersion of the primary below that of the subcluster, suggesting that the system is viewed shortly after core passage. In either case the high relative velocity of subcluster to the primary, 1940 km s^{-1} in the two-component fit and 1702 km s^{-1} in the three-component fit, is consistent with viewing a merger near the time of core passage (see, e.g., eq. [15] and associated discussion in Sarazin 2002).

A simple sanity check on the merger hypothesis is to ask whether the presumed merging parties are bound. Treating the primary and subcluster as point masses, the simple Newtonian condition for a bound system is

$$V_r^2 R_p \leq 2GM \sin^2\alpha \cos\alpha, \qquad (2)$$

where V_r is the line-of-sight velocity difference between the two masses, R_p is their projected separation, M is the total mass, and α is the projection angle defined from the plane of the sky. The KMM analysis provides a reference from which to evaluate this condition, in particular by providing estimates for V_r, R_p, and M (under the assumption that both the primary and the subcluster represent virialized systems). In the

two-component fit, $V_r = 1940$ km s^{-1}, $R_p = 700$ kpc, and $M = 3.4 \times 10^{15}\ M_\odot$ (the virial masses for the primary and subcluster are 2.1×10^{15} and $1.3 \times 10^{15}\ M_\odot$, respectively). Thus, the system is bound for nearly all projection angles ($6° \leq \alpha \leq 84°$). Only if the total mass of the system is very low ($\lesssim 8 \times 10^{14}\ M_\odot$) would the system be unbound. Similarly, using the two largest components in the three-component fit, the system would be bound for $5° \leq \alpha \leq 85°$ and unbound if $M \lesssim 5 \times 10^{14}\ M_\odot$. Note that in the latter case, the virial assumption is surely suspect as the subcluster has the larger velocity dispersion and hence implied mass ($0.9 \times 10^{15}\ M_\odot$ for the primary and $1.4 \times 10^{15}\ M_\odot$ for the subcluster).

This merger hypothesis is potentially further supported by the X-ray morphology, although as with the case of a simple superposition there are difficulties. The X-ray emission of the main body of A2125 is elongated in a direction perpendicular to the low surface brightness X-ray emission. This elongation is consistent with ''an initial coalescence of subunits of comparable masses'' (Wang et al. 1997), whereas at later stages the elongation would tend to be along the supercluster filament (see also the simulations of Roettiger et al. 1997). However, it is clear that the X-ray emission from the main body of A2125 represents only a small portion of the entire system (refer to Fig. 4). While a merger of some sort is indicated by the X-ray data, the scale of this merger is debatable.

In any case, we are observing A2125 under special circumstances that may largely explain some of the peculiarities of the cluster. At richness class 4, it is among the very richest clusters of galaxies known (e.g., Morrison et al. 2003). Similarly, its large velocity dispersion suggests that it is a massive cluster containing many galaxies. However, these factors are inconsistent with the low X-ray luminosity and temperature of the cluster ($L_X = 7.9 \times 10^{43}$ ergs s^{-1} and $T = 3.2$ keV; Wang et al. 2004). For example, using the σ-T relationship of Lubin & Bahcall (1993), the velocity dispersion of A2125 would predict a temperature of 7.5 keV. Such a discrepancy can be explained if the system is composed of multiple complexes seen in projection, whether these components are merging or not. A more appropriate application of the σ-T relationship would then be for an individual cluster in the system. Working backward, the X-ray temperature predicts a velocity dispersion of about 670 km s^{-1}, a figure in line with the velocity dispersions of the larger substructures (i.e., components with the most members) identified in the KMM analysis (refer to Table 6).

4.2. Emission-Line versus Non–Emission-Line Galaxies

As prior studies (e.g., Owen et al. 1999; Morrison et al. 2003) have noted an excess in the fraction of active galaxies in A2125 relative to other clusters of comparable richness, we performed a simple investigation of activity as defined by the presence of emission lines. For this purpose, the noted presence of any emission line in a galaxy's spectrum regardless of the strength of that line was sufficient for inclusion of that galaxy in the emission-line sample. Using this definition, 75 of 224 cluster galaxies (33.5%) were emission-line objects. Unfortunately, we lack comparable data sets for other intermediate-redshift clusters to test whether this fraction is unusually high. For comparison, 96 of the 151 noncluster galaxies in the field of A2125 (63.6%) were emission-line objects.

When measured over the entire cluster, the dynamics of the emission-line galaxies does not differ significantly from that of the non–emission-line galaxies. The systemic velocity and dispersion for the emission-line galaxies were $73,798 \pm 133$

and 1148^{+107}_{-84} km s^{-1}, respectively, while those for the non–emission-line galaxies were $73,950 \pm 90$ and 1092^{+70}_{-58} km s^{-1}. Similarly, there is no significant evidence that the emission-line galaxies are drawn from a different population than the cluster galaxies as a whole, as quantified by KS and Wilcoxon tests. The positional data suggest that the emission-line galaxies are at lower declinations, although this is significant only at $1.85\,\sigma$. We also checked whether the emission-line galaxies were preferentially associated with any substructures identified via the KMM analysis. A χ^2 test indicated that there was no statistical difference in the fraction of galaxies with emission lines among the various groups. Thus, the emission-line galaxies are fairly well mixed throughout the cluster.

5. CONCLUSIONS

We have reported on a program that has obtained 371 galaxy velocities in the direction of the $z = 0.2465$ rich cluster A2125. These new velocities include 222 cluster galaxies (including 25 in common with those reported in Owen et al. 1999), which increases the total number of confirmed cluster members to 224, making this among the better studied intermediate-redshift Butcher-Oemler clusters. The galaxy velocities were subjected to a large number of statistical tests that identified significant substructure. Through comparison with numerical simulations, these tests indicated that A2125

is consistent with a merger of comparable-mass clusters viewed along an axis within $\sim 30°$ of the merger axis. This merger is viewed within a few hundred million years of the time at which the cores of the respective components have crossed.

A favorable alignment of multiple structures, be they involved in a merger or simply seen in projection, is helpful in understanding the general properties of A2125. The combination of these structures produces an unusually high richness and velocity dispersion, reconciling the apparent discrepancy of the richness of the cluster with its low X-ray temperature and luminosity.

REFERENCES

Abell, G. O. 1958, ApJS, 3, 211
Abell, G. O., Corwin, H. G., & Olowin, R. P. 1989, ApJS, 70, 1
Ashman, K. M., Bird, C. M., & Zepf, S. E. 1994, AJ, 108, 2348
Bahcall, N. A., et al. 2003, ApJS, 148, 243
Beers, T. C., Flynn, K., & Gebhardt, K. 1990, AJ, 100, 32
Bird, C. M. 1993, Ph.D. thesis, Univ. Minnesota
Bird, C. M., & Beers, T. C. 1993, AJ, 105, 1596
Butcher, H., & Oemler, A. 1984, ApJ, 285, 426
Condon, J. J. 1992, ARA&A, 30, 575
Danese, L., de Zotti, G., & di Tullio, G. 1980, A&A, 82, 322
Dressler, A., & Shectman, S. A. 1988, AJ, 95, 985
Dwarakanath, K. S., & Owen, F. N. 1999, AJ, 118, 625
Fitchett, M. J. 1988, MNRAS, 230, 161
Helou, G., Soifer, B. T., & Rowan-Robinson, M. 1985, ApJ, 298, L7
Hill, J. M., & Oegerle, W. R. 1998, AJ, 116, 1529
Lubin, L. M., & Bahcall, N. A. 1993, ApJ, 415, L17

Miller, N. A., Owen, F. N., & Hill, J. M. 2003, AJ, 125, 2393
Morrison, G. E., Owen, F. N., Ledlow, M. J., Keel, W. C., Hill, J. M., Voges, W., & Herter, T. 2003, ApJS, 146, 267
Owen, F. N., Ledlow, M. J., Keel, W. C., & Morrison, G. E. 1999, AJ, 118, 633
Pinkney, J., Roettiger, K., Burns, J. O., & Bird, C. M. 1996, ApJS, 104, 1 (P96)
Roettiger, K., Loken, C., & Burns, J. O. 1997, ApJS, 109, 307
Sarazin, C. L. 2002, in Merging Processes in Clusters of Galaxies, ed. L. Feretti, M. Gioia, & G. Giovannini (Dordrecht: Kluwer), 1
Tonry, J., & Davis, M. 1979, AJ, 84, 1511
Wang, Q. D., Connolly, A. J., & Brunner, R. J. 1997, ApJ, 487, L13
Wang, Q. D., Owen, F., & Ledlow, M. 2004, ApJ, in press
West, M. J., & Bothun, G. D. 1990, ApJ, 350, 36
West, M. J., Oemler, A., & Dekel, A. 1988, ApJ, 327, 1
Yahill, A., & Vidal, N. V. 1977, ApJ, 214, 347
Yun, M. S., Reddy, N. A., & Condon, J. J. 2001, ApJ, 554, 803